

# Bat Bot 2.0: bio-inspired anisotropic skin, passive wrist joints, and redesigned flapping mechanism

Jonathan Hoff<sup>1</sup>, Nicole Jeon<sup>2</sup>, Patrick Li<sup>2</sup>, Joohyung Kim<sup>1</sup>

**Abstract**— Bat flight has been an underdeveloped area of bio-inspired robotics because of the vast complexities of biological bat flight and the over 40 degrees of freedom present in their bodies. The robotic flapping system Bat Bot (B2) has been shown to exhibit fundamental properties of biological bat flight with its articulated wings, its deformable membrane, and its controllable hindlimbs. However, the system is limited in performance by its relatively large mass for the thrust it produces. In an effort to further pursue this important area of flapping flight, we have made several important hardware improvements to the system based on biological inspiration. These include passive wrist joints to reduce negative lift in the upstroke and a novel elastic fiber membrane to mimic the anisotropic nature of bat skin for performance and durability. The redesigned flapping mechanism and structure have reduced the weight by 22%, increased the flapping amplitude, lowered mechanical slackness, and improved mass distribution. These hardware improvements are functional together in free-flight tests. This new system Bat Bot 2.0 (B2.0) provides insights into the important elements of design of bat robots, and it brings the goal of complex bat flight maneuvers closer to reality.

## I. INTRODUCTION

Numerous works in robotics have relied on biology for inspiration. Flapping flight is one of these areas that has seen significant growth in the past 10 years. There are insect-scale robots [1], [2], flapping-wing micro aerial vehicles (FWMAV) mimicking hummingbirds [3], [4], and other ornithopters that are larger in scale [5], [6]. Given the complexities of bat flight and their over 40 degrees of freedom (DoF) [7], there have been relatively fewer systems mimicking these creatures. Most notably, Bat Bot (B2) has successfully shown to mimic biology with its articulated wings, hindlimbs, and flexible membrane [8], [9], and it matches the kinematic synergies found in biology [10], [11].

Past works have begun to explore the area of flight planning and aerial maneuvers for B2 [12], and they have built accurate models of the system [13]. However, B2 is limited in its capability for complex flight maneuvers because of its low thrust-to-weight ratio. This particular size scale is difficult because of its relatively heavy morphing wings, the requirement for a robust actuation system to enable flapping, and the complexity in designing a material analogous to bat wing membrane. We desire to improve flight performance of this system to widen the area of flight maneuvers for this system and to identify the salient design elements of a bat

<sup>1</sup>Authors are with the Coordinated Science Laboratory and Department of Electrical and Computer Engineering, University of Illinois at Urbana-Champaign (UIUC), Urbana, IL 61801, USA.  
 jehoff2@illinois.edu

<sup>2</sup>Authors are with the Mechanical Science and Engineering Department, UIUC.

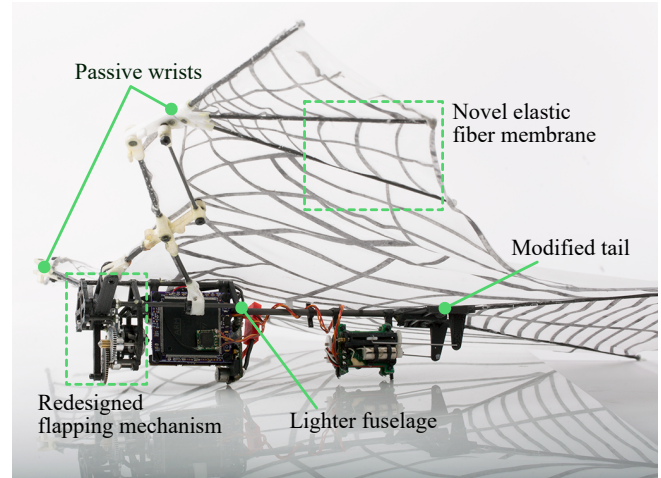


Fig. 1: B2.0 prototype.

robot. Thus, we first consider biology for inspiration and to find aspects of biology that are missing in this design. For example, biological bats have wing folding and bending in the upstroke [14], and they have anisotropic skin [15] with a complex elastin fiber network [16]. Additionally, their wings are capable of large flapping amplitudes up to 150° [17].

In this paper, we have designed the new prototype Bat Bot 2.0 (B2.0) with several major hardware improvements as shown in Figure 1. The updated gearbox and flapping mechanism have lowered the system's mass, increased the maximum wingbeat amplitude, reduced mechanism slackness, and improved the mass distribution. The redesigned frame reduced the mass of the system. B2.0's mass is 90 g compared to B2's mass of 116 g. We improved the wing by adding passive wrists that increase lift generation and still retain the folding and unfolding abilities. A novel bio-inspired elastic structure added to the membrane provided greater wing strength, thrust performance, and membrane durability. The tail was adjusted to maintain membrane tension at its extreme points of extension. We ran numerous load cell experiments to identify the effects of the design modifications, and we observed increased thrust performance from the new membrane, increase in lift because of the passive wings, and no thrust penalties with the new mechanism despite its reduced mass. Additionally, we tested B2.0 with all hardware improvements in preliminary free-flight experiments.

The paper is organized as follows. Section II provides a review of related works. We elaborate on the design and bio-

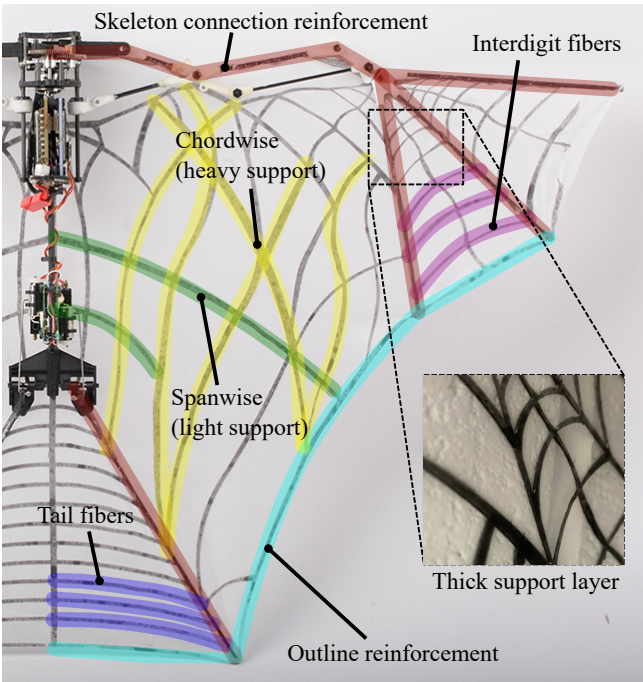


Fig. 2: Fabricated membrane with base layer (clear) glued to elastic fiber outline (black).

inspiration of the hardware improvements in Section III, and we discuss load cell tests, free-flight experiments, and results analysis in Section IV. Section V concludes the paper with a discussion of the study and proposes future work.

## II. BACKGROUND

Our design improvements for B2.0 build upon existing literature in the areas of wing folding, membrane design, and mechanism design for flapping systems.

### A. Wing folding

Past work studying biology proposed that bats fold their wings when flapping upwards to reduce parasitic lift and inertial costs [14]. Bahlman *et al.* [18] confirmed this hypothesis by designing and testing robotic bat wings with active folding. Additionally, Hoff *et al.* [11], [19] coupled wing folding with flapping with the robot B2 to reduce negative lift effects and inertial forces. However, many of the DoFs present in biology bats were actually fixed in B2, including the joints on the wrist. The carbon fiber rods for the digits were epoxied to the wrists. When flapping, the wings would pronate and supinate, i.e. twist about the spanwise direction. This passive bending would direct the force vector slightly forward, and it is responsible for thrust generation. However, there is no net lift generation because the wings are rigid and bend equally in the upstroke and downstroke.

Other works have experimented with passive wing folding to reduce negative lift generated in flapping systems. Mueller *et al.* [20] tested a solid hinge, Delrin hinge, and a carbon fiber rod hinge that each bend in the upstroke. Each improved lift, but there were some reductions in thrust. Wissa *et al.* [21] utilized a novel compliant spine for an ornithopter that used

less electric power, increased flapping frequency, and did not significantly decrease thrust generation. Other work has designed wings that passively unfold during flapping [22].

### B. Membrane design

The wing membrane of a bat plays an important role in its aerodynamics, most notably for its ability to mechanically change under varying flow conditions without additional energy input [23]. Schwartz *et al.* [24] observed that a typical bat wing consists of parallel bundles of collagen and elastin fibers. While collagen is known for its biomechanical tensile strength, the elastin fiber network was found to be primarily responsible for the wing's mechanical characteristics. Additionally, bat skin presents anisotropic behavior, showing the greatest stiffness strength in the chordwise direction (parallel to the body) and the greatest failure strain in the spanwise direction (perpendicular to the body) [15], [24]. While elastin fibers typically run in the spanwise direction, it is difficult to identify the exact function of the geometric patterns, as other bats have fibers concentrated in the chordwise direction [16]. It was also found that the tail membrane has the greatest load-bearing capacity in order to promote the development of an aerodynamic camber at the center of the wing, which is the weakest yet most extensible part of the wing [24].

There are relatively few works regarding replication of bat wing skin. Bahlman *et al.* [18] created a membrane from silicone and used 0.5 mm and 0.25 mm elastic threads to anchor it to a robotic bat wing, reduce billowing, and reinforce the leading and trailing edges. B2's membrane similarly was made from silicone and was attached directly to the wing skeleton [9]. This work also briefly mentioned use of embedded carbon fibers in the membrane [9].

### C. Flapping mechanism design

The flapping flight literature is filled with numerous examples of different flapping mechanism designs. Many works have utilized rigid link mechanisms such as the single drive gear and a crank-slider mechanism [25] and the dual crank-rocker design [26]. Others have used servo motors for flapping and have benefited from independent wing control and arbitrary wing trajectories [6], [18]. A few insect and hummingbird-size FWMAVs have used string-driven flapping mechanisms [3], [27]. These benefit from large flapping amplitudes, as there are no singularity points in the kinematics. Additional works have explored use of flapping mechanisms with springs that operate at resonant frequencies [25], [28]. Larger systems have utilized spatial four-bar crank-rocker mechanisms with ball-and-socket joints on either side of the frame to actuate the wings [21].

It is especially challenging to design a flapping mechanism for a robotic bat because biological bat wings are relatively heavier than other fliers. Likewise, B2's wings and membrane make up over 15% of its total weight. Thus, the system requires a robust mechanism to handle the large inertial loads. Past works have used servo motors [18] and a spatial four-bar crank rocker design [9] for flapping actuation.

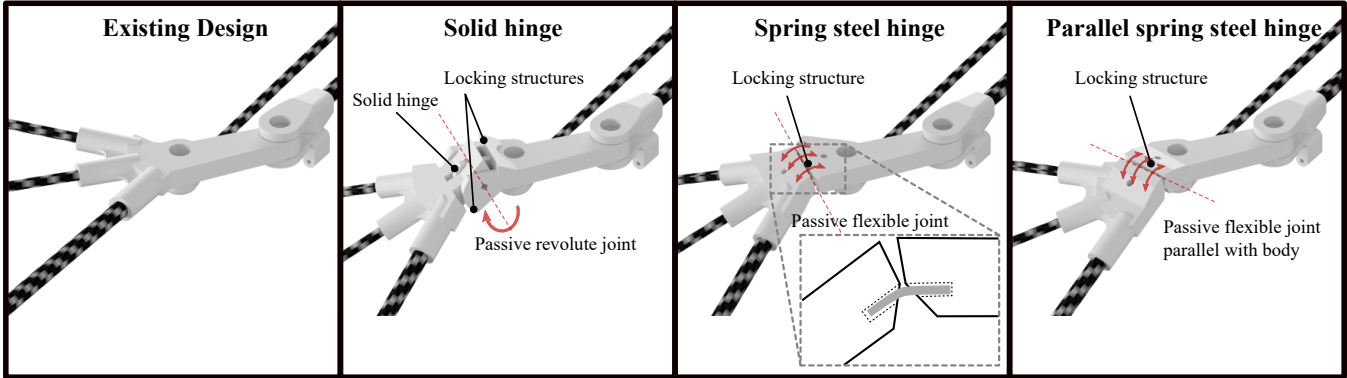


Fig. 3: Comparison of different passive hinge designs.

### III. HARDWARE IMPROVEMENTS

There are three primary hardware improvements presented in this paper. We have added a bio-inspired elastic fiber structure to support the membrane, passive wing folding at the wrist joints, and a redesign of the flapping mechanism and structure. The following sections detail these improvements.

#### A. Membrane

B2 used a thin (0.056 mm) silicone membrane that was stretched across the wings, body, and tail [9]. This allowed the wings to fold in and out while maintaining tension across the wings. However, this design came with some limitations. Most prominently, some areas of B2's membrane had significant billowing when flapping, and this reduced the thrust produced by the system. These areas required more support because of the higher aerodynamic loads. A thicker membrane would alleviate this issue, but it would greatly increase the total mass of the robot and reduce folding actuation because of the stiffness increase in the membrane. The membrane has also had issues with tearing at the connection points to the skeleton because of the high degree of strain on these points.

Drawing from biology for inspiration, we designed a secondary silicone layer (Figure 2) in a similar manner of elastin fiber networks from real bat morphology [16]. Since the greatest stiffness strength is observed chordwise in bats [15], [24], fibers in such direction were made to be the thickest and more numerous while spanwise fibers were the thinnest and fewest to mimic the anisotropic stiffness of bat skin. From a practical standpoint, this prevents folding and extending the wings from being inhibited while increasing the stiffness of the membrane for more force generation. The fiber network of the tail membrane was designed with a higher concentration of spanwise fibers to increase its load-bearing capacity for the development of the camber in the center of the wing [24]. Muscle fibers and neurovasculature were not considered since the robot cannot mimic muscle activation and articulation. Collagen fibers were also not considered since collagen does not significantly contribute to biomechanical function [23]. The membrane has had past challenges with tearing at the connection points on the

skeleton. Therefore, in order to reduce wear-and-tear due to concentrated stresses in the attachment points, we outlined the membrane with a border at all connection points for strength and durability.

Both layers were fabricated with Smooth-On Dragon Skin 10 SLOW. We mixed a lower proportion of silicone solvent in making the fiber layer in order to increase the thickness. A laser cutter was used to create the outline of the fiber network. The layers were then glued together with a mixture of silicone epoxy and solvent. A small amount of black silicone pigment was added to the epoxy for aesthetics. The thickness of the secondary layer is 0.33 mm, significantly thicker than the base layer (0.02 mm) in order to provide adequate support. The base layer has a mass of 14.19 g, and the fiber network has a mass of 5.68 g, combined for a total mass of 19.87 g. This is compared to the original membrane of B2 with a mass of 19.21 g.

#### B. Passive wing folding

We have developed a mechanism for passive folding that works in cooperation with the articulated armwing mechanism of the robotic bat. We combine elements of passive folding from past works while maintaining the morphing wing structure. Adding hinges at each finger joint would produce a more biologically sound design. However, these hinges need to be made very small, and consequently would be more prone to failure, have less stability, and increase the total mass. Therefore, we decided to add a single joint at each wrist that bends in one direction and is locked in the other. During every downstroke, the joint will remain rigid. During every upstroke, the joint will bend, reducing effective surface area and negative lift.

In an effort to select the most effect passive wing design for the robot, we designed three different folding mechanisms. Each is displayed in Figure 3. First, we created a solid hinge with three vertical supports on the side connecting to the armwing and two supports on the side attaching to digits. The additional support on each part provided less slackness in the hinge than using a two support and one support connection. Finally, we added a horizontal stopper on top of each hinge to fix the joint in place during the downstroke. A thin metal rod connected the two pieces together at the

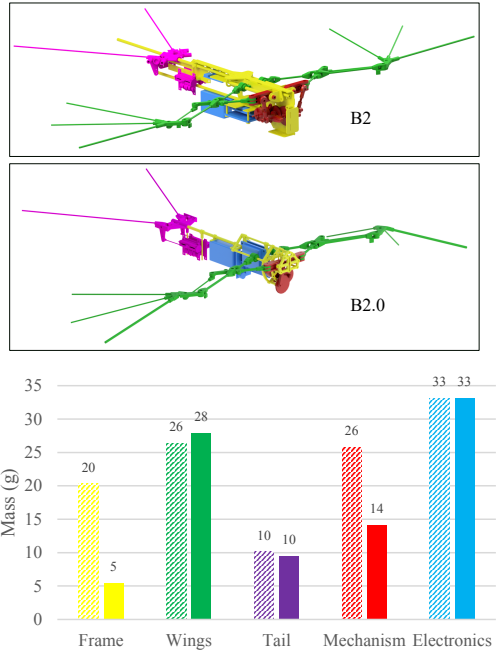


Fig. 4: Mass comparison of B2 (top) and B2.0 (middle). The plot (bottom) compares the mass breakdown of B2 in dashed bars and B2.0 in solid bars.

joint. We selected a  $35^\circ$  range of motion, as this was the angle that provided the most lift in [20].

Second, we considered a design with passive bending during the upstroke. The solid hinge was replaced with two spring steel plates 0.005 in thick and 0.25 in width. The spring steel hinge is displayed in Figure 3. The hinge is held in place with carbon fiber rods pushed through the holes on each side. This design is a mix between the solid hinge by Mueller *et al.* [20] and the compliant spine by Wissa *et al.* [21]. Energy will be stored in the wing during the upstroke and transferred to thrust at the beginning of the downstroke.

Third, we adapted the spring steel hinge design's bending axis to be parallel with the body when the wings are at maximum extension. Only one spring steel plate is used between the two components in order to compare a different spring constant. B2's original wrist was 0.59 g. The new designs each are slightly heavier as expected: the solid hinge is 1.00 g, the spring steel hinge is 0.95 g, and the spring steel hinge parallel to the body is 0.98 g.

### C. Tail

When the hindlimbs of B2 tilted up together, the distance between their ends would decrease because of their offset pivot angles of the revolute joints, thus reducing the tension of the surface and the aerodynamic effect it had on the system. The tail was redesigned such that the pivot axis of each hindlimb was made to be orthogonal to the body, while maintaining the angle between the hindlimbs and the body.

### D. Gearbox, flapping mechanism, and frame

The gearbox of B2 is shown in Figure 4. It used two steel spur gears and two brass pinions (pitch modulus 0.3 mm) with a total gear ratio of 30:1 between the brushless DC

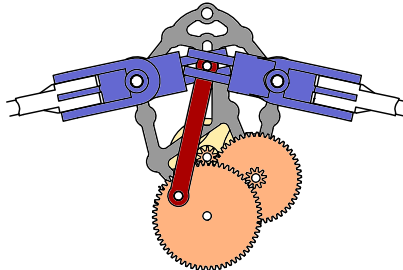


Fig. 5: B2.0 gearbox and flapping mechanism diagram.

(BLDC) motor and the drive shaft. The motor was attached on the right side of the frame. The 2-mm titanium drive shaft was attached to the drive gear, and aluminum crank arms were secured at the keyed ends of the shaft with set screws. Two metal collars held the drive shaft in place. The rotational motion of the crank arms drove the wings to rock back and forth, acting as a spatial four-bar crank-rocker mechanism. Ball-and-socket joints were used at the shoulder of the wing and the crank arm because the mechanism was non-planar; the crank and the rocker planes of rotation were orthogonal. The shoulder links of the wings were 3D-printed nylon parts that rotated on two aluminum plates.

1) *Mass:* There are several limitations to this design of B2. First and foremost, the mass of the flapping mechanism and frame could be reduced. Figure 4 displays the mass breakdown of the gearbox. The two aluminum cranks added 1.5 g to the system, the drive shaft added 0.4 g, and the drive shaft collars added 1.2 g. The flapping mechanism was non-planar and thus required ball-and-socket joints totaling 2.4 g in mass. Additionally, the drive shaft was relatively long (25.7 mm) and thus needed to be machined from titanium due to high torque loads that would bend a 2 mm steel shaft. The frame was constructed with 1/32 in carbon fiber plates epoxied together, carbon fiber tubes, and two aluminum shoulder plates to support the wings. These added 12.5 g to the mass.

2) *Limited flapping amplitude:* Second, the kinematics of the flapping mechanism were susceptible to mechanical singularity. Increasing the flapping amplitude was possible by increasing the crank arm attachment radius, however, this would lead to the mechanism sticking at the flapping position extrema. Increasing the length between the shoulder joint and the ball-and-socket connection improved this slightly, but it caused an increase in the length of both the shoulder parts and the drive shaft mechanism, thereby creating an even higher torque load on the shaft and heavier parts.

3) *Mechanism slackness:* Third, there was some slackness in the flapping mechanism. Because of the long drive shaft and its narrow connection points on the frame, the shaft could be loosened by the wings. For example, if one wing was held fixed and the system was driven to flapping, the result would be a larger flapping amplitude of the other wing and almost no movement of the held wing.

4) *Mass distribution:* Fourth, the BLDC motor contributed to asymmetry in mass distribution as it was posi-

tioned on one side of the frame. This may have affected flight behavior because of the CoM distribution of the system.

B2.0's gearbox, flapping mechanism, and frame build upon B2's design and improve each of these limitations. Figure 5 displays the gearbox and mechanism, and Figure 4 shows the new frame. The same BLDC motor and metal gears as B2 are housed in a 1 mm thick aluminum frame. The gears spin on 1.5 mm steel shafts on flanged steel bearings press fit in the frame. Three 2 mm carbon fiber tubes create the structure for the frame and attach the aluminum frame to a 3D-printed front frame piece. The 3D-printed parts for the frame use the Markforged Onyx filament, a nylon with chopped carbon fibers. The carbon fiber sides running the length of the body were removed, and only the 3 mm carbon fiber tube remains connecting the tail to the frame. The tail servo motors are mounted to this rod with 1.5 mm carbon fiber tubes. The electronic speed controller (ESC), receiver, microprocessor, and inertial measurement unit (IMU) are mounted to the inner chassis with two hooks and glue. The battery is attached to the tube between the tail and fuselage.

The wings are attached to 3D-printed shoulder links that pivot about these tubes. The drive gear connects to the other ends of the shoulders with a 3D-printed coupler link. The end of the link has a orthogonal 1.5 mm carbon fiber rod that extends between the two frame pieces and slides in the open groove on each side. This rod also slides between four other carbon fiber tubes extending out of the shoulder links. This sliding design reduces mechanical singularity because of the sliding connection between the coupler link and the shoulder links, as this was a ball-and-socket joint on B2. B2's mechanism had flapping amplitudes of 17° in the upstroke and 18.5° in the downstroke, and B2.0's mechanism has amplitudes of 27.5° in the upstroke and 25.6° in the downstroke. One of the biggest design challenges was preventing the gears from skipping because of the high inertial loads from the wings and aerodynamic forces pushing the gears apart. We added a rear 3D-printed frame piece with two bearings to provide additional support for the gear shafts to alleviate this issue.

The mass breakdown of the system is shown in Figure 4. The largest mass reductions were the flapping mechanism and the frame, with 15 g removed from the frame and 12 g from the gearbox and flapping mechanism. Wing mass increased slightly because of the passive wrists and the slightly heavier membrane. Electronics remain the same because nothing was modified. In total, B2.0 has a mass of 90 g compared to B2's total mass of 116 g, a 22% reduction. We will note that the version of B2 used in this paper has a higher mass than past works [8], [9] because additional mechanical changes were necessary to improve robustness of the gearbox and flapping mechanism (steel gears, ball-and-socket joints, bearings, etc.) to prevent failures in the mechanism.

#### IV. EXPERIMENTS

We evaluated the performance improvements of each of the hardware modifications from Section III by recording

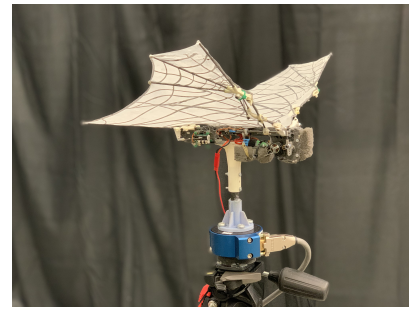


Fig. 6: Load cell experiments configuration with B2 structure and flapping mechanism.

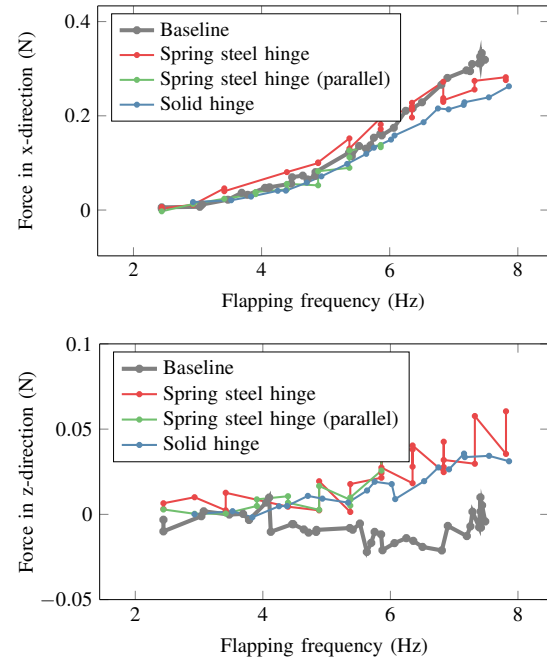


Fig. 7: Load cell results of the average thrust and lift forces for flapping with existing wings and with passive wrist wings.

force data on a load cell while flapping the robot's wings. We focused our analyses on the thrust ( $x$ ) and lift ( $z$ ) forces generated from flapping at various speeds.

##### A. Load cell tests

In order to capture the effects of each hardware addition, we individually tested each addition on the load cell for flapping at varying frequencies. An analog six-axis JR3 force-torque sensor (model #30E12A4) recorded the force data. The resolution was 0.005 N in the  $x$ ,  $y$  axes and 0.01 N in the  $z$  axis. A dSPACE CLP1104 I/O box and DS1104 R&D Controller Board sampled the sensor's signals at a rate of 1000 Hz. We secured B2 to the sensor with a carbon fiber tube connected between a mount on the load cell and a mount on the robot as shown in Figure 6. The load cell was secured to a tripod for stability. We supplied a fixed voltage of 8.4 V to power the ESC and BLDC motor that drive flapping on the robot. The current to the motor was changed by hand via a radio transmitter in order to vary the flapping frequency.

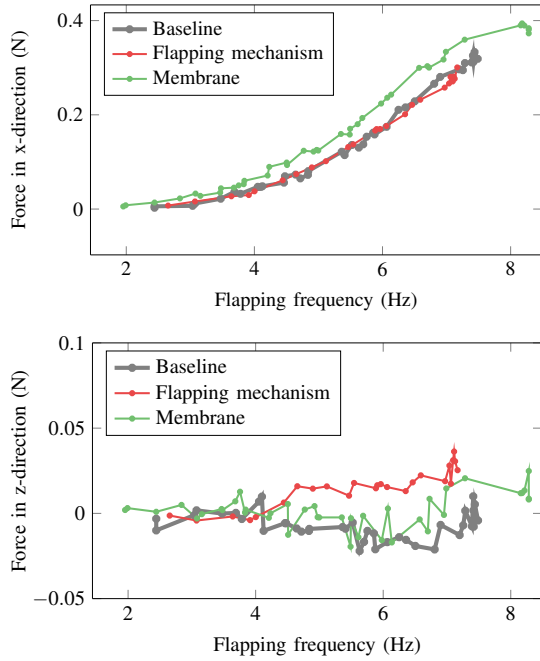


Fig. 8: Load cell results of the average thrust and lift forces for flapping with existing wings, with new membrane, and with new flapping mechanism.

The throttle setting was held constant for each test.

We post-processed the force data in the  $x$  and  $z$  directions using MATLAB by subtracting the nominal force readings (no flapping) to remove the force of gravity and sensor biases. Then, we removed high frequency noise using a 6<sup>th</sup>-order Butterworth low-pass filter with a cutoff frequency of 50 Hz. For a given recording, we selected a range of approximately 2 s to include only an integer number of flapping periods such that the average of the data was not biased positively or negatively.

We recorded experiments with the previous system B2 (existing wings, membrane, and flapping mechanism) in order to get a baseline measurement. Then, we individually substituted the different additions of the three passive wing designs, the membrane, and the flapping mechanism and ran tests with each. The passive wing and membrane tests used B2's flapping system in order to accurately compare the individual differences with the baseline. The new flapping mechanism test required B2.0's frame and mechanism, and thus it was run with a different set of wings and membrane.

The tests include six different hardware configurations and for total of  $N_l = 163$  recordings. Flapping frequencies varied between 2 Hz to 8.5 Hz. We recorded 39 baseline tests, 26 spring steel hinge tests, 14 parallel spring steel tests, 19 solid hinge tests, 25 flapping mechanism tests, and 40 membrane tests. There were the fewest parallel spring steel tests because the hinge broke after 14 tests. Using only one spring steel piece made the wrist significantly weaker.

## B. Results

We used two metrics to evaluate the performance of each hardware configuration. The average force in the  $x$  direction

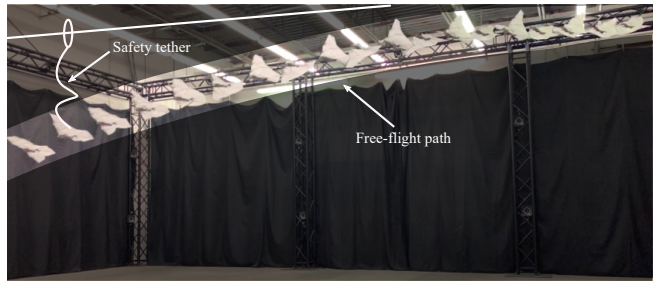


Fig. 9: A free-flight experiment with B2.0 for a duration of 2 s.

provides a strong indicator of thrust production of the robot, and the average force in the  $z$  direction informs the lift generation of the system. These averages are computed as

$$\bar{F}_x^i = \frac{1}{M_i} \sum_{k=1}^{M_i} F_x^i(t_k), \quad \bar{F}_z^i = \frac{1}{M_i} \sum_{k=1}^{M_i} F_z^i(t_k) \quad (1)$$

where  $M_i$  is the last point of data with the same phase as the start point.  $F_x^i(t_k)$  and  $F_z^i(t_k)$  are the forces in the  $x$  and  $z$  directions for trial  $i$  at time sample  $k$ . The frequency of each test is computed by finding the peak locations of  $F_z^i$  and finding the average period between them.

We compare the results of the different passive wing configurations in Figure 7. Each of the passive wing configurations outperformed the baseline for lift generation. The passive wings generated more net positive lift because folding in the upstroke reduced negative lift. The spring steel hinge generated the most thrust and lift of the three passive wings. It had minimal thrust penalties at higher frequencies compared with the baseline. Interestingly, it generated more thrust for lower flapping frequencies than the baseline. The solid hinge lost the most thrust of the three designs. The parallel hinge's performance tracked that of the solid hinge, though it wore out before reaching higher frequencies.

The flapping mechanism and membrane comparison with the baseline appears in Figure 8. The new flapping mechanism matched the thrust of the baseline despite its reduced mass. The net lift was also improved as well, possibly from the larger flapping amplitude, though the underlying cause is difficult to identify. The most significant improvement was seen by the new membrane load cell tests on the B2 hardware system. Across all frequencies, the thrust is noticeably improved. Additionally, B2 was able to reach higher flapping frequencies, possibly because the membrane puts less stress on the system compared with the single thicker layer membrane of B2's design. In summary, the load cell tests demonstrate improvements for each of the design elements tested.

## C. Free-flight tests

In order to test the design elements in flight, we assembled B2.0 with the new flapping mechanism, frame, passive wings, membrane, and tail (Figure 1). We performed free-flight tests by launching the robot by hand and controlling the throttle and tail manually with a transmitter. The robot was powered with a small 2S LiPo battery. A thin safety tether

attached to the robot's frame prevented it from hitting the ground at the end of the flight tests. The tether was connected loosely to a taught string above spanning the length of the room. The tether could slide along the string with minimal friction, and it did not affect the flight of the robot because it was slack during the flight portion of the tests.

Figure 9 displays one of the flight tests. The robot maintained lateral stability during the flight. The passive wings, membrane, and mechanism did not induce unstable modes in the system. B2.0's design improvements were functional together to propel the robot in free-flight. More flight experiments will be undertaken to examine the performance differences between B2.0 and B2.

## V. CONCLUSIONS

The previous hardware platform B2 was limited by its relatively heavy mass, as it is challenging to mimic the articulation in biological bats with the current state of technology. The reduction in weight and improvement in performance for B2.0's design are the next steps paving the way for more complex flight maneuvers for robotic bats. They increase the thrust-to-weight ratio which is critical for maneuvers, and they provide more lift generation.

While the hardware improvements successfully performed all the experiments and test flights, we found some components which can be improved. For example, the teeth on the brass pinion gear between the small gear and drive gear began to wear out after prolonged flapping time because of the high inertial loads. The parallel hinge also wore out because of using only one spring steel layer. We will continue to develop the hardware improvements and make efforts to reduce the weight.

Redesigning the bat robot B2 has given insights into new areas of research. There are numerous avenues to pursue regarding the design of the membrane. Adjusting different parameters like thickness, placement of spanwise and chordwise fibers, and different reinforcement materials would further improve performance. More efforts can be undertaken to explore the design space of the passive wings such as the spring constant and the maximum bending angle.

## REFERENCES

- [1] X. Deng, L. Schenato, W. C. Wu, and S. S. Sastry, "Flapping flight for biomimetic robotic insects: Part I-system modeling," *IEEE Transactions on Robotics*, vol. 22, no. 4, pp. 776–788, 2006.
- [2] K. Y. Ma, P. Chirarattananon, S. B. Fuller, and R. J. Wood, "Controlled flight of a biologically inspired, insect-scale robot," *Science*, vol. 340, no. 6132, pp. 603–607, 2013.
- [3] M. Keenon, K. Klingebiel, and H. Won, "Development of the nano hummingbird: A tailless flapping wing micro air vehicle," in *50th AIAA Aerospace Science Meeting*, 2012, p. 588.
- [4] J. Zhang, F. Fei, Z. Tu, and X. Deng, "Design optimization and system integration of robotic hummingbird," in *IEEE International Conference on Robotics and Automation (ICRA)*. IEEE, 2017, pp. 5422–5428.
- [5] A. A. Paranjape, S.-J. Chung, and J. Kim, "Novel dihedral-based control of flapping-wing aircraft with application to perching," *IEEE Transactions on Robotics*, vol. 29, no. 5, pp. 1071–1084, 2013.
- [6] J. Gerdes, A. Holness, A. Perez-Rosado, L. Roberts, A. Greisinger, E. Barnett, J. Kempny, D. Lingam, C.-H. Yeh, H. A. Bruck, et al., "Robo Raven: a flapping-wing air vehicle with highly compliant and independently controlled wings," *Soft Robotics*, vol. 1, no. 4, pp. 275–288, 2014.
- [7] D. K. Riskin, D. J. Willis, J. Iriarte-Díaz, T. L. Hedrick, M. Kostandov, J. Chen, D. H. Laidlaw, K. S. Breuer, and S. M. Swartz, "Quantifying the complexity of bat wing kinematics," *Journal of Theoretical Biology*, vol. 254, no. 3, pp. 604–615, 2008.
- [8] A. Ramezani, X. Shi, S.-J. Chung, and S. Hutchinson, "Bat Bot (B2), a biologically inspired flying machine," in *IEEE International Conference on Robotics and Automation (ICRA)*. IEEE, 2016, pp. 3219–3226.
- [9] A. Ramezani, S.-J. Chung, and S. Hutchinson, "A biomimetic robotic platform to study flight specializations of bats," *Science Robotics*, vol. 2, no. 3, pp. eaal2505, 2017.
- [10] J. Hoff, A. Ramezani, S.-J. Chung, and S. Hutchinson, "Synergistic design of a bio-inspired micro aerial vehicle with articulated wings," in *Robotics: Science and Systems*, 2016.
- [11] ———, "Optimizing the structure and movement of a robotic bat with biological kinematic synergies," *The International Journal of Robotics Research*, vol. 37, no. 10, pp. 1233–1252, 2018.
- [12] J. Hoff, U. Syed, A. Ramezani, and S. Hutchinson, "Trajectory planning for a bat-like flapping wing robot," in *IEEE/RSJ International Conference on Intelligent Robots and Systems (IROS)*. IEEE, 2019, pp. 6800–6805.
- [13] J. Hoff and S. Hutchinson, "Data-driven modeling of a flapping bat robot with a single flexible wing surface," in *Robotics: Science and Systems*, 2020.
- [14] D. K. Riskin, A. Bergou, K. S. Breuer, and S. M. Swartz, "Upstroke wing flexion and the inertial cost of bat flight," *Proceedings of the Royal Society of London B: Biological Sciences*, vol. 279, no. 1740, pp. 2945–2950, 2012.
- [15] S. Swartz, J. Iriarte-Diaz, D. Riskin, X. Tian, A. Song, and K. Breuer, "Wing structure and the aerodynamic basis of flight in bats," in *45th AIAA Aerospace Sciences Meeting and Exhibit*, 2007, p. 42.
- [16] J. A. Cheney, J. J. Allen, and S. M. Swartz, "Diversity in the organization of elastin bundles and intramembranous muscles in bat wings," *Journal of Anatomy*, vol. 230, no. 4, pp. 510–523, 2017.
- [17] R. Bullen and N. McKenzie, "Scaling bat wingbeat frequency and amplitude," *Journal of Experimental Biology*, vol. 205, no. 17, pp. 2615–2626, 2002.
- [18] J. W. Bahlman, S. M. Swartz, and K. S. Breuer, "Design and characterization of a multi-articulated robotic bat wing," *Bioinspiration & Biomimetics*, vol. 8, no. 1, p. 016009, 2013.
- [19] J. Hoff, A. Ramezani, S.-J. Chung, and S. Hutchinson, "Reducing versatile bat wing conformations to a 1-dof machine," in *Living Machines*, 2017.
- [20] D. Mueller, J. W. Gerdes, and S. K. Gupta, "Incorporation of passive wing folding in flapping wing miniature air vehicles," in *ASME Mechanism and Robotics Conference*. American Society of Mechanical Engineers, 2009, pp. 797–805.
- [21] A. Wissa, Y. Tummala, J. Hubbard Jr, and M. Frecker, "Passively morphing ornithopter wings constructed using a novel compliant spine: Design and testing," *Smart Materials and Structures*, vol. 21, no. 9, p. 094028, 2012.
- [22] A. K. Stowers and D. Lentink, "Folding in and out: Passive morphing in flapping wings," *Bioinspiration & Biomimetics*, vol. 10, no. 2, p. 025001, 2015.
- [23] J. A. Cheney, N. Konow, A. Bearnott, and S. M. Swartz, "A wrinkle in flight: the role of elastin fibres in the mechanical behaviour of bat wing membranes," *Journal of the Royal Society Interface*, vol. 12, no. 106, p. 20141286, 2015.
- [24] S. Swartz, M. Groves, H. Kim, and W. Walsh, "Mechanical properties of bat wing membrane skin," *Journal of Zoology*, vol. 239, no. 2, pp. 357–378, 1996.
- [25] S. S. Baek, K. Y. Ma, and R. S. Fearing, "Efficient resonant drive of flapping-wing robots," in *IEEE/RSJ International Conference on Intelligent Robots and Systems (IROS)*. IEEE, 2009, pp. 2854–2860.
- [26] G. De Croon, M. Perçin, B. Remes, R. Ruijsink, and C. De Wagter, "The Delfly," *Springer*, vol. 10, pp. 978–94, 2016.
- [27] D. Gong, D. Lee, S. Shin, and S. Kim, "String-based flapping mechanism and modularized trailing edge control system for insect-type FWMAV," *International Journal of Micro Air Vehicles*, vol. 11, 2019.
- [28] J. Zhang, B. Cheng, J. A. Roll, X. Deng, and B. Yao, "Direct drive of flapping wings under resonance with instantaneous wing trajectory control," in *IEEE International Conference on Robotics and Automation (ICRA)*. IEEE, 2013, pp. 4029–4034.